Particulate-matter Diameter Estimation Based on Mie Light Scattering Method for Atmospheric Pollution

Hariyanto
Department of Electrical Engineering, Universitas Indonesia

Ucuk Darusalam
Faculty of Information and Communications Technology, Universitas Nasional

Purnomo Sidi Priambodo
Department of Electrical Engineering, Universitas Indonesia

https://doi.org/10.5109/7326974

出版情報：Evergreen. 11 (4), pp.3383-3389, 2024-12. Interdisciplinary Graduate School of Engineering Sciences, Kyushu University, Japan
バージョン：

EVERGREEN Joint Journal of Novel Carbon Resource Sciences & Green Asia Strategy, Vol. 11, Issue 04, pp3383-3389, December, 2024

Particulate-matter Diameter Estimation Based on Mie Light Scattering Method for Atmospheric Pollution

Hariyanto[1], Ucuk Darusalam[2], Purnomo Sidi Priambodo[1,*]
[1]Department of Electrical Engineering, Universitas Indonesia, Depok 16424, Indonesia
[2]Faculty of Information and Communications Technology, Universitas Nasional, Jakarta 12520, Indonesia

*Author to whom correspondence should be addressed:
E-mail: purnomo.sidhi@ui.ac.id

(Received December 4, 2023; Revised March 28, 2024; Accepted November 25, 2024).

Abstract: Particulate matter (PM) is a crucial component of air pollution found in both indoor and outdoor (ambient) environments. PM not only poses a risk to human health and driving safety but also plays a role in the transmission of Covid-19. In this study, we propose a novel approach-the Mie scattering method-to estimate the PM diameter. This method involves the scattering of laser light on spherical particles at various angles, providing a unique perspective on PM analysis. The results of our research simulations demonstrate a direct correlation between the scattering angle and the scattered light-to-illumination intensity ratio. We also observed that varying particle diameter leads to changes in I_S/I_0. In our experiment, we varied the particle diameter from 0.2 to 0.5 µm, aligning with the general atmospheric pollution conditions PM2.5. Analysis of the I_S/I_0 ratio at certain scattering angles and wavelengths can be used to estimate the diameter of light-scattering spherical particles. The I_S/I_0 value increases as the particle size increases. Varying wavelength values affect changes in I_S/I_0; as the wavelength increases, the I_S/I_0 value becomes lower. The simulation results conclude that the optimal angle for scattering observations is between angles 0^0 and 40^0.

Keywords: Particulate-Matter diameter; Air Pollution; Mie Scattering; Laser Light; Scattered Light; Wavelength; Scattering Angle

1. Introduction

The existence of air pollution is characterized by the release of substances into the atmosphere that surpass the established limit and pose a threat to human health and other biological entities, and it causes environmental degradation. The air pollutant substances can be gases such as carbon monoxide, ammonia, nitrous oxide, methane, chlorofluorocarbons, particulates (organic and inorganic), or biological molecules[1,2]. Air pollution inside or outside the room (ambient) can be caused by chemical gases, biological substances, or dust particles, which change the natural properties of the atmosphere. One of the dangerous pollutant elements is dust particles, which are also called particulate matter (PM). The mixture of solid particles and water droplets in the air is an example of PM. Moreover, PM can be classified into two categories based on its diameter: PM2.5 refers to particles with sizes below 2.5 µm, also known as smooth PM, and PM10 encompasses particles ranging from 2.5 to 10 µm in size, often referred to as coarse PM[3].

PM can be found outdoors and indoors. PM in ambient can be sourced from motor vehicle pollution, forest fires, and volcanic eruptions. PM in the room can be produced from cigarette smoke, air circulation disturbances (ventilation), and smoke originating from the cooking process in the kitchen[3].

Natural sources of atmospheric pollution originating from land and sea are generally PM10, for example, volcanic eruptions. Meanwhile, the source of atmospheric pollutant PM2.5 is a secondary product of this natural process. Atmospheric pollution has increased enormously in the last few decades because many community activities produce pollution that exceeds that caused by natural events. Some examples of atmospheric pollution due to community activities are the usage of various non-renewable fossil-based energy sources[4]. The common sources of PM are diesel engines[5], biomass[6] and coal combustion[7]. Those are widely used in various industry types as the PM emission sources, which causing air pollution.

Many countries are aware of the importance of environmental health by implementing policies to reduce the PM emission of diesel engines. There are three kinds of policies to reduce PM emission[8], first by reducing the number of diesel engines, the second by implementing a silver-based catalyst[9], and the third is the development of a new asymmetrical rotating combustion technique, which is formulated to function in flameless mode. It possesses a remarkably uniform temperature distribution and reduced levels of pollutant emissions. These attributes render it suitable for clean and efficient combustion engines[10].

PM can potentially exert detrimental impacts on human health. Various human ailments have been linked to the contamination of PM, encompassing untimely mortality, heart attacks, irregular cardiac rhythm, exacerbated asthmatic episodes, diminished pulmonary capabilities, and respiratory manifestations[11-14]. The impact of particle size on the toxicity effect is of considerable significance. As particle diameter decreases and the total particle surface area increases, particle toxicity also increases[15]. PM can also cause the spread of the COVID-19 virus because of the possibility of a correlation between PM and the diffusion of the COVID-19 virus so that airborne spread becomes easier[16]. Additionally, the scattering and absorption of light by PM can reduce visibility[4),17-18] and subsequently impact the safety and security of driving. Engine components like gas turbine propellers at high temperatures and speeds can also experience damage due to PM, which can cause larger disasters[19]. Environmental conditions can also be problematic if exposed to PM. The problems caused include changes in the earth's radiation balance, cloud formation, and increasing global warming[20,21].

Several techniques are available to analyze the concentration of PM and its size, based on optical scattering, optical absorption, pollutant mass gravity, and microbalance oscillations techniques.

The principles of scattering, absorption, and extinction of light can be used to measure particle concentration in real time on optical instruments[22]. Other PM monitoring is based on gravity by collecting particles in a filter within a time interval. The weight of the particles in the filter is then compared to the volume of air collected from the ambient air[23,24], using the principle beta reduction[25], the tapered element oscillating microbalance[26], surface acoustic wave mass sensor[27], and microfabricated air-microfluidic sensor[28].

Below, we review several research results regarding PM measurement methods based on light scattering methods. Aerosol particles illuminated by a beam of light will continue or scatter this light in all directions (scattering). Li et al.[29] compared the calculation of electromagnetic scattering in partially charged spherical particles using Rayleigh approximation and Mie theory where Mie theory is more suitable for calculating the scattering of charged spherical particles.

Zi Ye et al.[30] measured the particle size distribution using a mathematical model based on Mie scattering theory through light scattering intensity and introduced a stochastic inversion algorithm based on Markov chains to improve the accuracy and noise immunity of particle size distribution measurements. The numerical simulations show that the Markov chain algorithm has strong noise immunity and can meet the online measurement requirements for particle size distribution.

Chen et al.[31] in their research used an integrated light scattering method to measure the concentration of particulate matter in situ. A real-time particle concentration measurement system is created by studying the effects of particle size and the best detection angle. Mie scattering theory calculates the sensitivity of the mass concentration of five common particles with aerodynamic sizes between 0.05 – 10 μm by applying different scattering angles.

Chen et al.[32] also proposed a method for measuring the mass concentration of particulate matter for homogeneous spherical particles using light scattering. The technique employs two types of sensors, one stationary in the forward direction and the other rotating. Measurements are carried out in real-time. Particle mass concentration is measured with a fixed detector, and the particle size is measured from the intensity ratio of the detectors. The results were compared with particles measured with an electric low-pressure impactor (ELPI).

Jobert et al.[33] described the development of a miniature particulate matter sensor for personal air quality monitoring. This sensor works based on Lorenz Mie's theory used to model the light scattering by spherical particles. The sensor uses a visible fibrous light source and a perforated retinal image sensor to measure particle scattering signatures, the detection, and the differentiation of particles of different sizes.

Han et al.[34] used laser angular scattering by analyzing the difference in particle size sensitivity between forward and backward scattering to measure the mass concentration of particulate matter online. This method uses angular scattering of the laser and three fixed detectors to improve the accuracy of mass concentration measurements.

This research aims to estimate the diameter of PM based on the Mie light scattering method. This is a theoretical simulation research using MATLAB software, where there are three parameters involve in this analysis, i.e.: wavelength (λ), particle diameter (a) and scattering angle (θ). The three parameters are varied and the output are variations of the I_S/I_O ratio versus scattering angles. For fixed illumination wavelength, the larger the pollutant size, the greater the scattering intensity. Moreover, for fixed observation angle and fixed particle diameter, the longer the illumination wavelength, the smaller the scattering intensity. These simulation results help us to select the most effective illumination wavelengths for various particle sizes.

2. Methods

In the analysis, PM size is analyzed by using Mie Scattering method with a scattering approach to a single spherical object, as shown in Fig. 1 below. The assumption of a single spherical object based on the following concept. When the particle concentration are not too dense, it can be assumed that their collective scattering as a large number of independent scatterings. This results in a scattering curve of only a few multiples of the curve for a single sphere[35].

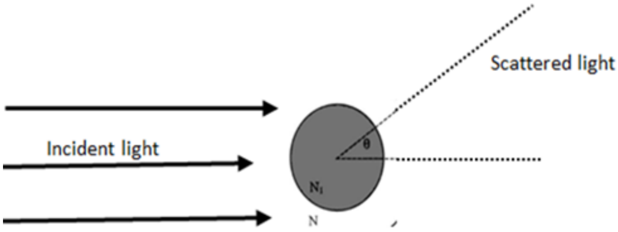

Fig. 1: The Mie scattering on the surface of spherical particles, where *N* is the refractive index of the medium, N_1 is the particle refractive index, and θ is the scattering angle.

When incoming light illuminates a spherical particle surface , the light is scattered, and the intensity scattering distribution angle can be described using Mie's theory for the scattered electric field, as represented by Eq. 1[36,37]. Mie Theory is a mathematical model that describes the scattering of electromagnetic waves by spherical particles. The Mie's theory involves the particle size, particle and medium refractive indices, the scattered particle shapes, illuminating wavelength, and polarization of the incident light. This allows us to estimate the size of the scattering sphere, by comparing the measured angular scattering distribution with the theoretical distribution for a single sphere[35].

$$E_S = \sum_{n=1}^{\infty} E_n \left(i a_n N_{eln}^{(3)} - b_n M_{oln}^{(3)} \right),$$
$$H_S = \frac{k}{\mu\omega} \sum_{n=1}^{\infty} E_n \left(i b_n N_{oln}^{(3)} + a_n M_{eln}^{(3)} \right), \tag{1}$$

where $N_{eln}^{(3)}$ and $M_{oln}^{(3)}$ are the 3rd kind of spherical harmonic vectors, E_n is the incident electric field amplitude of the first kind Legendre order *n*, and a_n and b_n are Mie scattering field expansion coefficients. The coefficients a_n and b_n can be obtained by Eq. 2[37].

$$a_n = \frac{\mu m^2 j_n(mx)[x j_n(x)]' - \mu_1 j_n(x)[mx j_n(mx)]'}{\mu m^2 j_n(mx)\left[x h_n^{(1)}(x)\right]' - \mu_1 h_n^{(1)}(x)[mx j_n(mx)]'},$$
$$b_n = \frac{\mu_1 j_n(mx)[x j_n(x)]' - \mu j_n(x)[mx j_n(mx)]'}{\mu_1 j_n(mx)\left[x h_n^{(1)}(x)\right] - \mu h_n^{(1)}(x)[mx j_n(mx)]}, \tag{2}$$

The spherical Bessel function of the first type is j_n, h_n represents the spherical Hankel function, and x signifies the particle size parameter as defined in Eq. 3[37]:

$$x = \frac{2\pi a}{\lambda} m_{medium} \tag{3}$$

$$m = \frac{m_{sphere}}{m_{medium}}$$

where λ represents the illuminating wavelength (nm), *a* is the particle diameter (μm), m_{sphere} represents the refractive index sphere, m_{medium} represents the medium refractive index, and *m* is the refraction relative index.

The other functions encompass the functions π_n and τ_n[37], deemed as the angular eigenfunctions that elucidate the scattering pattern of spherical harmonic vectors. These functions depend on the scattering angle, θ, as shown in Eq. 4, below.

$$\pi_n = \left[\frac{2n-1}{n-1}\cos(\theta) . \pi_{n-1}\right] - \left[\frac{n}{n-1} . \pi_{n-2}\right] ,$$
$$\tau_n = [n\cos(\theta) . \pi_n] - [(n+1) . \pi_{n-1}] , \tag{4}$$

The value of the initial condition is determined by Eq. 5.

$$\pi_0 = 0 \quad \pi_1 = 1 \quad \pi_2 = 3\cos(\theta) ,$$
$$\tau_0 = 0 \quad \tau_1 = \cos(\theta) \quad \tau_2 = 3\cos(2\theta), \tag{5}$$

We can analyze the angular scattering amplitudes of S_1 and S_2 with the relationship in Eq. 6[37].

$$S_1 = \sum_{n=1}^{n_{max}} \frac{2n+1}{n(n+1)} (a_n \pi_n + b_n \tau_n)$$
$$S_2 = \sum_{n=1}^{n_{max}} \frac{2n+1}{n(n+1)} (a_n \tau_n + b_n \pi_n) \tag{6}$$

If the association between the amplitude of the scattering angles S_1, S_2 and the scattering intensity function i_1, i_2 is known, according to Eq. 7.

$$i_1 = |S_1|^2$$
$$i_2 = |S_2|^2 \tag{7}$$

If there is incident light, then the light is scattered by particles, then the light will be partially polarized so that the intensity of the I_S scattering light can be expressed by Eq. 8[30].

$$I_S = I_0 \frac{\lambda^2}{8\pi^2 r^2} (i_1 + i_2) \tag{8}$$

The initial light intensity is I_o, and *r* represents the distance from the sensor to the particle.

3. Result and discussion

The simulation is using Matlab program to calculate the values of a_n, b_n, π_n, and τ_n based on Eq. 2, 3, 4, 5, and 6 and the available Matlab function[38].

Table 1. The simulation parameters used in the analysis.

Parameter	value
λ	650 nm
r	15 cm
Diameter (a)	0,26 µm
Medium refractive index (m_{medium})	1 + 0i
Particle refractive index (m_{sphare})	1.33 - 0i

As shown in Table 1, the illuminating wavelength (λ) is a visible light source 650 nm. The approximate distance from the sensor to the particle is 15-cm, the distance is chosen for convenience in experiment. The chosen particulate diameter is 0.26 µm, which is in the range of PM2.5. The refractive index of the air medium is 1 - 0i and the refractive index of water droplets is 1.33 + 0i[31]. Imaginary values indicate absorption, if the imaginary value is zero, it means there is no absorption occurs. The simulation carried out in this paper includes four items, as follows:

3.1 Mie angular scattering.

Used to calculate the magnitude of the Mie scattering intensity matrix S_1 and S_2 with the value of u = cos(θ) and display it in a polar diagram with S_1 in the upper half circle for ($0 < \theta < 180^0$) conversely S_2 is in the lower half circle for ($180^0 < \theta < 360^0$)[38], so the simulation results are obtained as shown in Fig. 2.

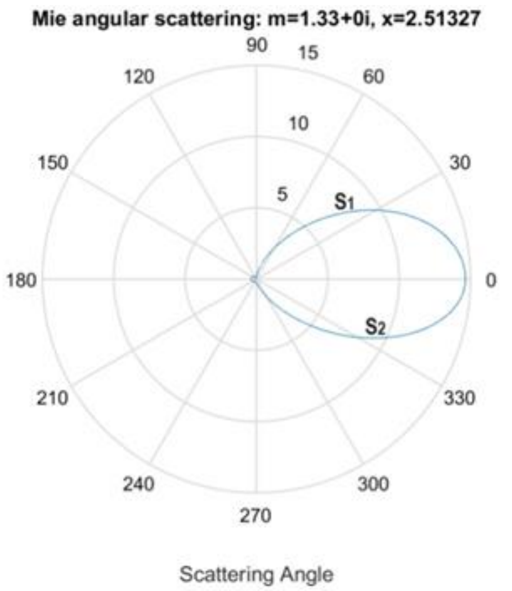

Fig. 2: The association curve between $|S_1|^2$ (upper curve) and $|S_2|^2$ (lower curve) versus the scattering angles.

The data used in the simulation of Fig. 2 are based on data in Table 1. The value m = 1.3300 and the value x = 2.5133 are obtained by Eq. 3, where Fig. 2 is then calculated by Eq. 6. The angle variation distribution amplitude values of the scattering angles S_1 and S_2 are spread between 0 and 14. where the value S_1 plot is located above the semicircle, while S_2 plot is located below the semicircle.

3.2 The intensity ratio (I_S/I_O) versus scattering observation angles

In this case, the parameters of λ, r, a, m_{medium}, and m_{sphare} are set to be constants as shown in Table 1, and then I_S/I_O is obtained as a function of the scattering observation angles, where it is shown in Fig. 3 below.

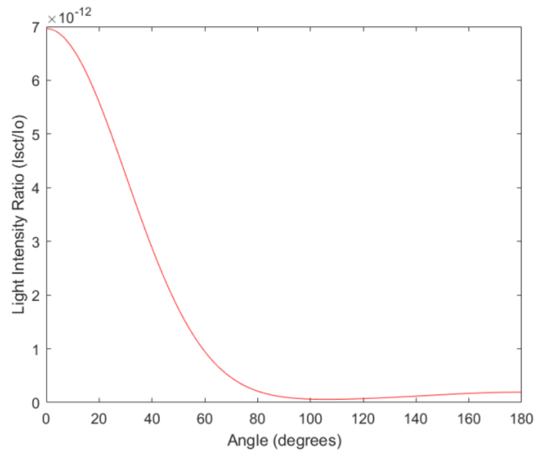

Fig. 3: The graph of the I_S/I_O ratio versus scattering angle.

The data used in the simulation of Fig. 3 are based on data in Table 1. The values of x = 2.5133 and m = 1.3300 are obtained by Eq. 3, where the graph of Fig. 3 is resulted by Eq. 7 and combined with Eq. 8. Figure 3 shows that the I_S/I_O ratio value decreases as the change in angle value increases. The steepest decline occurs when the angle value is between ($0^0 - 90^0$), the graphs display a period of relative flatness after this.

3.3 The intensity ratio (I_S/I_O) versus scattering observation angles with various particle diameters and fixed illumination wavelength.

In this case, the parameters of λ, r, a, m_{medium}, and m_{sphare} are set to be constants as shown in Table 1, and then I_S/I_O is obtained as a function of the scattering observation angles, where it is shown in Fig. 4 below. The next step is varying the particle diameter a with the following values of 0.2, 0.3, 0.4 and 0.5 µm. With respect to the change of a, it results into various x values, i.e.: 1.9333, 2.8999, 3.8666, and 4.8332 respectively, and m = 1.3300. Fig. 4 below shows 4 different plots with respect to each particle diameter value. The plots are calculated based on Eq. 7 and combined with Eq. 8.

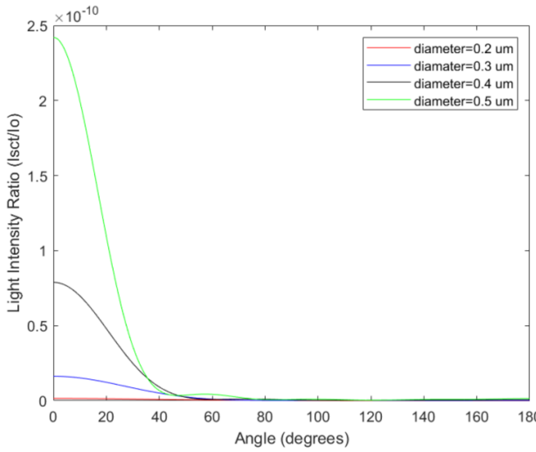

Fig. 4: The graph of the I_S/I_O ratio versus scattering angle, with different particle diameters and fixed illumination wavelength.

Figure 4 shows that the size of the particle diameter influences the I_S/I_O ratio value. When particle diameter increase, the I_S/I_O ratio value will also increase in common. The scattering observation angles between 0^0 and 40^0 show rapid I_S/I_O ratio change, and it is suggested to be the optimum angle area to be used for observation sensor position.

3.4 The intensity ratio (I_S/I_O) versus scattering observation angles with various illumination wavelengths and fixed particle diameter

In this case, the parameters of λ, r, a, m_{medium}, and m_{sphare} are set to be constants as shown in Table 1, and then I_S/I_O is obtained as a function of the scattering observation angles, where it is shown in Fig. 5 below. The next step is varying the illumination wavelength λ with the following values of 600, 650, 700, and 750-nm. With respect to the change of λ, it results into various x values, i.e.: 2.7227, 1.9333, 1.7952, and 1.6755 respectively, and m = 1.3300. Figure 5 below shows 4 different plots with respect to each illumination wavelength. The plots are calculated based on Eq. 7 and combined with Eq. 8.

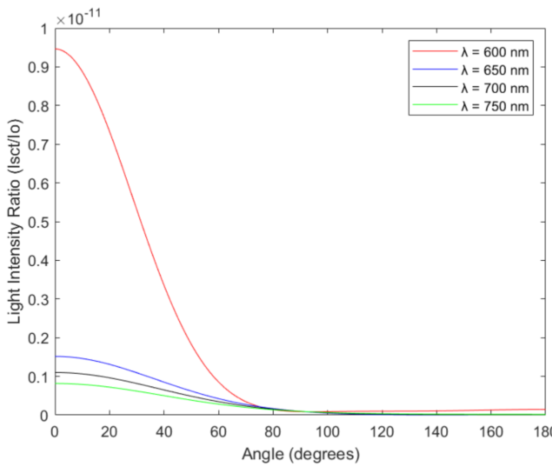

Fig. 5: The graph of the I_S/I_O ratio versus scattering angle, with different illumination wavelengths and fixed particle diameter.

Figure 5 shows that the longer illumination wavelength decreases the gradient change of the I_S/I_O ratio. This can be clearly observed in the observation scattering angles from 0^0 to 40^0. In common sense, a larger gradient is suggested for effective scattering observation. It is concluded that the use of shorter wavelengths will give more effective observation.

4. Conclusion

This research aims to analyze and estimate the size of pollution particles in the atmosphere. The technique used is electromagnetic scattering in the optical region, and the analytical approach is based on Mie scattering theory. The scattering formula successfully summarized was then used to simulate with MATLAB software.

From the results of various simulation variations, the following practical implications can be drawn, enhancing our understanding of atmospheric pollution:

1. As explained in simulation case #3, the larger the particle size, the easier it is to observe.
2. The shorter the illumination wavelength, the more effective it will be in analyzing particle size estimates, as described in simulation case #4.
3. As described in the simulation experiments for cases #3 and #4, the optimal scattering observation angle range is from 0^0 to 40^0. It is recommended that the observation sensor be placed at this angle range.

Acknowledgements

We thank the Meteorology, Climatology, and Geophysics Agency (BMKG) for the scholarship.

This research was funded by UNIVERSITAS INDONESIA for “Hibah Publikasi Terindeks Internasional (PUTI) Q2, Tahun Anggaran 2023–2024, Nomor: NKB-826/UN2.RST/HKP.05. 00/2023.

Abbreviations

PM = Particulate matter.

I_S/I_O = The intensity ratio of scattered light intensity and laser light.

References

1) O.R. Shaltami, N.M. Hamed, F.F. Fares, and H. Errishi, “Air pollution – a review virtual conference on environment and health (vceh) venue : agricultural university of iceland date : 4 october 2020 proceeding book,” *Virtual Conf. Environ. Heal. Venue Agric. Univ. Icel.*, 19 (*October*) 17–43 (2020).
2) N.A. Lestari, “Reduction of co_2 emission by integrated biomass gasification-solid oxide fuel cell combined with heat recovery and in-situ co_2 utilization,” *Evergreen*, 6(*3*) 254–261 (2019). doi:10.5109/2349302
3) Anonymous, “Particulate matter | air & radiation | us epa,” *US Environ. Prot. Agency*, (n.d.).

https://www.epa.gov/pm-pollution/particulate-matter-pm-basics#PM (accessed June 6, 2023).

4) W.S. Won, R. Oh, W. Lee, S. Ku, P.C. Su, and Y.J. Yoon, "Hygroscopic properties of particulate matter and effects of their interactions with weather on visibility," *Sci. Rep.*, 11 (*1*) 1–12 (2021). doi:10.1038/s41598-021-95834-6.
5) D. Sugeng, W. Yahya, A. Ithnin, B. Kusdi, M.A. Abdul Rashid, I. Bahiuddin, N. Mazlan, and H. Kadir, "Experimental comparison of smoke opacity and particulate matter emissions with the use of emulsion fuel," *Evergreen*, 7(3) 452–457 (2020). doi:10.5109/4068626.
6) Y. Furutani, K. Norinaga, S. Kudo, J. Hayashi, and T. Watanabe, "Current situation and future scope of biomass gasification in japan," *Evergreen*, 4(4) 24–29 (2017). doi:10.5109/1929681.
7) M.S. Alam, A.T. Wijayanta, and K. Nakaso, "Predictions of o2/n2 and o2/co 2 mixture effects during coal combustion using probability density function," *J Nov. Carbon Resour Sci*, 2 12–16 (2010).
8) T. Sato, "How is a sustainable society established? : a case study of cities in japan and germany," *Evergreen*, 3(2) 25–35 (2016). doi:10.5109/1800869.
9) H. Ruan, M. Nishibori, T. Uchiyama, K. Kamitani, and K. Shimanoe, "Soot oxidation activity of ag/hzsm-5 (si/al=40) catalyst," *Evergreen*, 4(2/3) 7–11 (2017). doi:10.5109/1928668.
10) A.S. Najib Aminu Ismail, Mazlan Abdul Wahid, Aminuddin Sa'at, "A review on the combustion characteristics of an asymmetric swirling combustor in flameless mode," *Evergreen*, 10(*3*) 1522–1537 (2023). doi:10.5109/7151700
11) G. Oberdörster, E. Oberdörster, and J. Oberdörster, "NANOTOXICOLOGY: an emerging discipline evolving from studies of ultrafine particles," *Environ. Health Perspect.*, 113 823–839 (2005). doi:10.1289/ehp.7339.
12) Y. Bai, R.E. Brugha, L. Jacobs, J. Grigg, T.S. Nawrot, and B. Nemery, "Carbon loading in airway macrophages as a biomarker for individual exposure to particulate matter air pollution — a critical review," *Environ. Int.*, 74 32–41 (2015). doi:https://doi.org/10.1016/j.envint.2014.09.010.
13) S. Rafael, L. Tarelho, A. Monteiro, E. Sá, A.I. Miranda, C. Borrego, and M. Lopes, "Impact of forest biomass residues to the energy supply chain on regional air quality," *Sci. Total Environ.*, 505 640–648 (2015). doi:https://doi.org/10.1016/j.scitotenv.2014.10.049.
14) K.-H. Kim, E. Kabir, and S. Kabir, "A review on the human health impact of airborne particulate matter," *Environ. Int.*, 74 136–143 (2015). doi:https://doi.org/10.1016/j.envint.2014.10.005.
15) A.D. Maynard, and E.D. Kuempel, "Airborne nanostructured particles and occupational health," *J. Nanoparticle Res.*, 7 (*6*) 587–614 (2005). doi:10.1007/s11051-005-6770-9.
16) Y. Zhu, J. Xie, F. Huang, and L. Cao, "Association between short-term exposure to air pollution and covid-19 infection: evidence from china," *Sci. Total Environ.*, 727 138704 (2020). doi:10.1016/j.scitotenv.2020.138704.
17) S. Tiwari, G. Pandithurai, S.D. Attri, A.K. Srivastava, V.K. Soni, D.S. Bisht, V. Anil Kumar, and M.K. Srivastava, "Aerosol optical properties and their relationship with meteorological parameters during wintertime in delhi, india," *Atmos. Res.*, 153 465–479 (2015). doi:https://doi.org/10.1016/j.atmosres.2014.10.003.
18) Y. Li, Q. Chen, H. Zhao, L. Wang, and R. Tao, "Variations in pm10, pm2.5 and pm1.0 in an urban area of the sichuan basin and their relation to meteorological factors," *Atmosphere (Basel).*, 6 150–163 (2015). doi:10.3390/atmos6010150.
19) S. Kumar, Akash, A. K.C, and K. Jayappa, "Solid particle erosion performance of multi-layered carbide coatings (wc-sic-cr_3c_2)," *Evergreen*, 10(2) 813–819 (2023). doi:10.5109/6792833.
20) A.S. Pipal, and P. Gursumeeran Satsangi, "Study of carbonaceous species, morphology and sources of fine (pm2.5) and coarse (pm10) particles along with their climatic nature in india," *Atmos. Res.*, 154 103–115 (2015). doi:https://doi.org/10.1016/j.atmosres.2014.11.007.
21) W. Gong, M. Zhang, H. ge, X. Ma, and Z. Zhu, "An investigation of aerosol scattering and absorption properties in wuhan, central china," *Atmosphere (Basel).*, 6 503–520 (2015). doi:10.3390/atmos6040503.
22) S.S. Amaral, J.A. de Carvalho, M.A.M. Costa, and C. Pinheiro, "An overview of particulate matter measurement instruments," *Atmosphere (Basel).*, 6 (*9*) 1327–1345 (2015). doi:10.3390/atmos6091327.
23) K.R. Spurny, "Methods of aerosol measurement before the 1960s," *Aerosol Sci. Technol.*, 29 (*4*) 329–349 (1998). doi:10.1080/02786829808965573.
24) A. Budianto, R. Wirawan, R. Illahi, D. Kurniawidi, S. Rahayu, and A.A. Kusuma, "A gravimetry-based fine particle concentration measurement system for humid environment using graphene oxide layer," *Evergreen*, 10(3) 1414–1421 (2023). doi:10.5109/7151690.
25) W. Chueinta, and P.K. Hopke, "Beta gauge for aerosol mass measurement," *Aerosol Sci. Technol.*, 35 (*4*) 840–843 (2001). doi:10.1080/027868201753227398.
26) G.P. Ayers, M.D. Keywood, and J.L. Gras, "TEOM vs. manual gravimetric methods for determination of pm2.5 aerosol mass concentrations," *Atmos. Environ.*, 33 (*22*) 3717–3721 (1999). doi:10.1016/S1352-2310(99)00125-9.
27) D. Nardi, E. Zagato, G. Ferrini, C. Giannetti, and F. Banfi, "Design of a surface acoustic wave mass sensor in the 100 ghz range," *Appl. Phys. Lett.*, 100 (2013). doi:10.1063/1.4729624.

28) I. Paprotny, F. Doering, P.A. Solomon, and M. Richard, "Microfabricated air-microfluidic sensor for personal monitoring of airborne particulate matter : design , fabrication , and experimental results," (n.d.).
29) X. Li, L. Xie, and X. Zheng, "The comparison between the mie theory and the rayleigh approximation to calculate the em scattering by partially charged sand," *J. Quant. Spectrosc. Radiat. Transf.*, 113 (*3*) 251–258 (2012). doi:10.1016/j.jqsrt.2011.09.020.
30) Z. Ye, X. Jiang, and Z. Wang, "Measurements of particle size distribution based on mie scattering theory and markov chain inversion algorithm," *J. Softw.*, 7 (*10*) 2309–2316 (2012). doi:10.4304/jsw.7.10.2309-2316.
31) D. Chen, X. Liu, J. Han, M. Jiang, Y. Xu, and M. Xu, "Measurements of particulate matter concentration by the light scattering method: optimization of the detection angle," *Fuel Process. Technol.*, 179 (*July*) 124–134 (2018). doi:10.1016/j.fuproc.2018.06.016.
32) D. Chen, X. Liu, J. Han, M. Jiang, Z. Wang, and J. Qi, "A new angular light scattering measurement of particulate matter mass concentration for homogeneous spherical particles," *Sensors (Switzerland)*, 19 (*10*) 18–20 (2019). doi:10.3390/s19102243.
33) G. Jobert, P. Barritault, M. Fournier, S. Boutami, A. Marchant, J. Michelot, P. Monsinjon, P. Lienhard, and S. Nicoletti, "Miniature particulate matter counter and analyzer based on lens-free imaging of light scattering signatures with a holed image sensor," *Sensors and Actuators Reports*, 2(1) 100010 (2020). doi:10.1016/j.snr.2020.100010.
34) J. Han, X. Liu, M. Jiang, Z. Wang, and M. Xu, "A novel light scattering method with size analysis and correction for on-line measurement of particulate matter concentration," *J. Hazard. Mater.*, 401 (*July 2020*) 123721 (2021). doi:10.1016/j.jhazmat.2020.123721.
35) I. Weiner, M. Rust, and T.D. Donnelly, "Particle size determination : an undergraduate lab in mie scattering particle size determination : an undergraduate lab in mie scattering," *American Journal of Physics*, 69(2) 129–136 (2001). doi: 10.1119/1.1311785.
36) H.C. Hulst, and H.C. van de Hulst, "Light scattering by small particles," Courier Corporation, 1981.
37) C.F. Bohren, "Absorption and scattering of light by small particles," *Absorpt. Scatt. Light by Small Part.*, (1983). doi:10.1088/0031-9112/35/3/025.
38) C. Mätzler, "MATLAB functions for mie scattering and absorption," *IAP Res Rep*, 2002–08 (*July 2002*) 1139–1151 (2002). http://arrc.ou.edu/~rockee/NRA_2007_website/Mie-scattering-Matlab.pdf.